International Journal of Computing and Digital Systems
ISSN (2210-142X)
Int. J. Com. Dig. Sys. 12, No.1 (Aug-2022)

https://dx.doi.org/10.12785/ijcds/120151

BatStateU Integrated Response Drone (BIRD): A Hybrid Unmanned Vehicle for Disaster Response

Ralph Gerard B. Sangalang *[1], **Oliver Lexter July A. Jose**[1], **Antonette V. Chua**[1] **and Janice F. Peralta**[1]

[1]*Department of Electronics Engineering, Batangas State University, Batangas City, Philippines 4200*

Received 30 Jan. 2021, Revised 19 Apr. 2022, Accepted 15 Jul. 2022, Published 6 Aug. 2022

Abstract: Drones, or Unmanned Aerial Vehicles (UAVs), are already being utilized to help people in need worldwide. In this report, the authors designed an unmanned vehicle composed of a flight mechanism & power supply, frame, and different payloads for different missions. These also include the design of different landing gears that are mechanically replaceable depending on the mission. This method allowed the drone to move in multi-mission or other environments (ground, air, and surface water) in normal conditions by changing its landing gears. A mapper payload that performs image stitching is also presented. The drone has an average flight time of 15 minutes, 4 *kg.* weight and can support payload weighing 5 *kg.*, it was tested to operate at a maximum altitude of 100 *m.* It can communicate through a remote controller via radio frequency signals. It can land and take off in ground and surface water and maneuver in different environments; air, ground (flat area), and surface water, depending on the attached payload. The tests were conducted in remote and actual environments given the three different landing gears, and the results show that the drone is ready for a real mission. Future payloads such as a medical kit and detachable communications links are considered for the next phase.

Keywords: Hexacopter Drone, BIRD, mapper, Unmanned Surface Vehicle, hybrid drone, BatStateU

1. Introduction

The Philippines placed second among countries reported in [1] that is greatly affected by tropical cyclones and extratropical storms in the past decade. There is a total of 333 storms that have affected the Philippines since 1960, which makes the country the most affected in Asia [1]. The country is 52.46 percent exposed to natural hazards, making it 53.85 percent vulnerable to disasters. There is a 33.35 percent susceptibility or likelihood that a severe catastrophe or natural disaster will cause significant damage, loss, and disruption to the country. In terms of risk, 'extreme weather events' is the top 3 risk identified in the insight report of the World Economic Forum 2022 [2].

With the level of risk to a disaster of the Philippines, preparedness, response, prevention & mitigation, and rehabilitation and recovery become a significant challenge for the national government. Various government and commercial agencies have launched projects and programs to minimize the country's risk and susceptibility to natural disasters.

Drones, or Unmanned Aerial Vehicles (UAVs), are already being used in humanitarian response worldwide [3], [4]. An unprecedented number of small and lightweight UAVs were launched in the Philippines after Super Typhoon Yolanda (internationally known as Typhoon Haiyan) in 2013 [5], [6]. It is the most promising and powerful new technology to improve emergency management during disaster response and relief operations. Drones naturally complement traditional manned relief operations by providing relief workers with better situational awareness and locating survivors amidst the rubble. It can also perform structural analysis of damaged infrastructure, evacuate casualties, and deliver needed supplies & equipment [7], [8].

During a crisis, preparedness and reaction are critical aspects, and new technology has demonstrated inventive and effective ways to carry out these tasks. In a disaster, roads may be in rubble or flooded, communication means may be down, and supplies & services such as medical service should be delivered quickly [9]. Unmanned vehicles (UVs) can be utilized to carry out these activities in isolated areas [4].

Unmanned aerial vehicles have four main application areas, namely:

1) mapping and remote sensing
2) search and rescue
3) transportation
4) training.

*R. G. B. Sangalang is the corresponding author. This project is part of the university priority projects on disaster response and mitigation provided by Batangas State University.

E-mail address: ralphgerard.sangalang@g.batstate-u.edu.ph, oliverlexterjuly.jose@g.batstate-u.edu.ph, antonette.chua@g.batstate-u.edu.ph, janice.peralta@g.batstate-u.edu.ph

Several works have been reported on the use of drones for different applications [3], [7], [8], [9], [10], [11], [12], [13], [14].

One key design aspect of unmanned vehicles is the control to be implemented during flight. An effective and cost-efficient design procedure is through the use of simulation software. By implementing this, a model of the vehicle can be made in software that can visualize the vehicle such as AutoCAD and SOLIDWORKS. These models can be imported to another simulation software to do the physics of flight simulation without diving into the entire range of equations. Several previous works have reported on the models [15], [16], [17] and control algorithm [18], [19], [20], [21] of an air vehicle.

One of the projects of Batangas State University is the BatStateU Integrated Response Drone (BIRD). It is the design and development of a ground/aerial/water surface Unmanned Vehicle system for immediate disaster response and monitoring. Specifically, these areas would be electromechanical, ground control station architecture, electronics control, and mapper payload.

Fig. 1 and Fig. 2 show the BIRD system overview and functional diagram, respectively. The hexacopter drone will be designed first before creating the control system. It will be the baseline for creating the plant model (drone) to be controlled. From this, the physics of flight will determine the mathematical definition of the drone's motion.

Referring to Fig. 2, the BIRD is packaged as a top-down functionality approach. The entire drone comes in a single transportation mode with the attachment payload in a separate package. The main drone contains support equipment such as the air vehicle frame, the on-board electronic control system (ECS), and other system interfaces such as the motors & sensors. Inside the ECS are the on-board hardware and the software for the flight control.

2. Methodology

There are three phases of the design of the UAV proposed. The drone is designed first to create the plant model required to design and simulate the controller. The payloads are designed to parallel with the controller. There are three different payloads for the UAV: water surface landing gear, land transport landing gear, and mapping payload. Fig. 3 shows the conceptual framework for the proposed design, and Fig. 4 shows the methodology followed while doing the design.

A. Drone Design

The aerodynamics and mechanical structure of the drone were considered during the design phase. The thrust generated by the propeller and motor was ensured to be enough to lift based on the selection of motor and propeller with a high thrust capability.

SOLIDWORKS is used to design the different frames of the drone. Simulations through finite element analysis were done using different frame materials resulting in carbon fiber with the best strength to weight ratio. Thus, drone frames were fabricated using carbon fiber material.

The maximum lift of the hexacopter is set at 9 *kg.*, including its weight and the other additional payload. The propeller and the motor determined the 9 *kg.* lift.

Equation (1) is used to calculate the lift and *rpm*, here a spinning propeller creates a pressure lower than the free stream in front of it and higher than the free stream behind it. The pressure downstream of the disk gradually returns to free-flowing conditions.

$$F_{lift} = \frac{1}{2}\rho\frac{\pi d^2}{4}(v_e^2 - v_o^2) \tag{1}$$

The drone must have the capability to move and land in air, water, and ground employing different landing gear designs. The landing gear determined and gave the drone the capability to move on different surfaces such as air, water, and ground. Thus, designing and combining different landing gear in one system gives flexibility but requires more lift force. Landing gears are independent and need an adopter to connect and reconnect to the drone.

B. Controller Design

The controller design is the top-level physical representation of the control system. It is composed of a processing unit and a wireless module to communicate with the ground station and payloads. The control system is divided into two sectors based on its functional purpose. These are Basic and Mission. In the Basic sector, the control system performs navigational tasks. In the Mission sector, the control is the link between the mission in which the air vehicle is commissioned to do. The processor unit performs parallel tasks threads that are mainly divided into two sections; Flight Processing and Mission Processing. The Flight Processing threads perform commands such as take-off, land, hover, etc. The Mission Processing threads perform mission-specific tasks based on the command sent by the ground station.

There are three main processes in the design of the controller: the plant model, controller model, and the environment model. Each component of the designed drone is drawn using a 3D drawing software, SOLIDWORKS. Each component drawn in SOLIDWORKS is then imported in MATLAB© Simulink© SimScape© Multibody. The drone is then remodeled using SimScape© Multibody. By this method, the software will be responsible for the drone's model as well as linearizing it. It eliminates the extremely difficult mathematical modeling of the drone and provides a higher-level model than most equations literature can give.

The equations of the physics of flight are used to model the controller. Although the hexacopter has the same number of actuators with its movement, it still is an under-

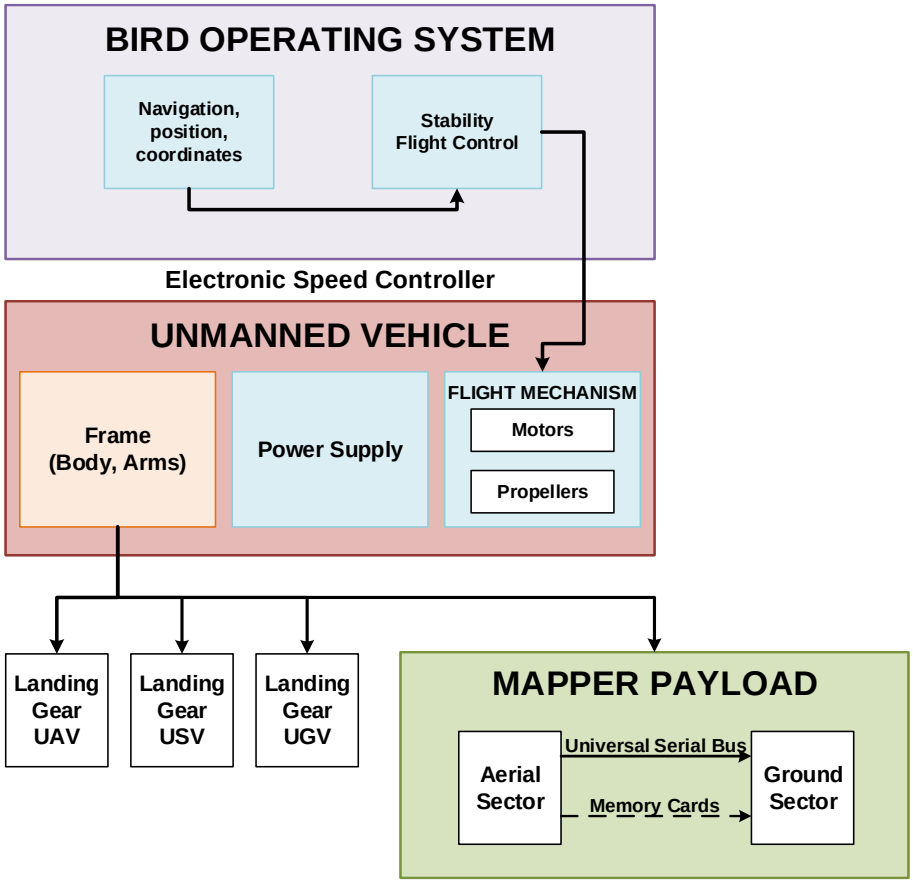

Figure 1. BIRD system overview consists of operating system, unmanned vehicle, landing gears and payload.

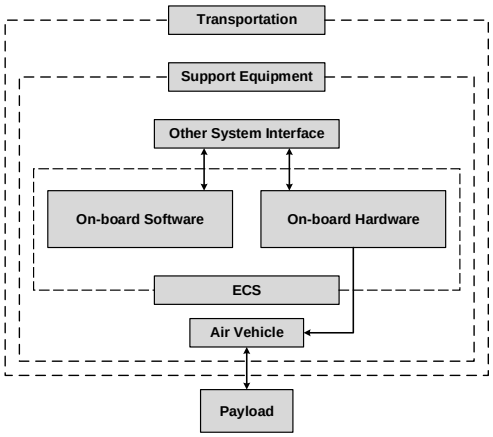

Figure 2. BIRD functional diagram

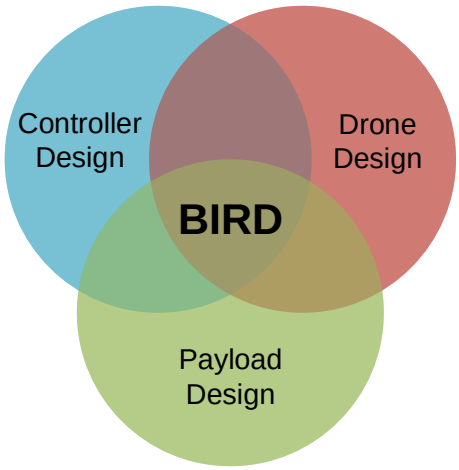

Figure 3. BIRD conceptual framework

actuated system. So, the two rotors contribute only to the thrust output of the drone.

The flight algorithm is based on the Newton-Euler equations [15] since the air vehicle is a hexacopter drone, (2) and (3) present the kinematics equations of the model.

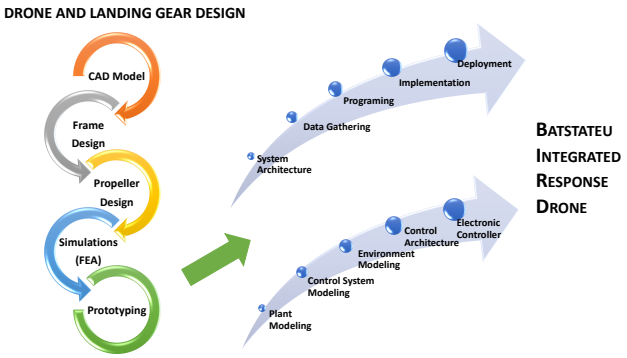

Figure 4. BIRD design methodology

$$\begin{bmatrix} \dot{x}_B \\ \dot{y}_B \\ \dot{z}_B \end{bmatrix} = A(\psi, \theta, \phi) \begin{bmatrix} V_x \\ V_y \\ V_z \end{bmatrix} \tag{2}$$

$$\begin{aligned} \dot{\psi} &= \frac{\omega_y \cos\phi}{\cos\theta} \\ \dot{\theta} &= \omega_z \cos\phi + \omega_y \sin\phi \\ \dot{\phi} &= \omega_x - (\omega_y \cos\phi - \omega_z \sin\phi) tg\theta \end{aligned} \tag{3}$$

where $A(\psi, \theta, \phi)$ is the rotation coordinate matrix of the air vehicle in a non-moving coordinate system; x_B, y_B, z_B are the air vehicles' coordinates; V_x, V_y, V_z are the linear speed components; ψ is the yaw angle; θ is the pitch angle; ϕ is the roll angle; ω_x,ω_y, ω_z are the air vehicle's angular velocities.

The translational motion model is described in (4),

$$\begin{cases} m(\dot{V}_x + \omega_y V_z - \omega_z V_y) &= F_x \\ m(\dot{V}_y + \omega_z V_x - \omega_x V_z) &= F_y \\ m(\dot{V}_z + \omega_x V_y - \omega_y V_x) &= F_z \end{cases} \tag{4}$$

where m is the air vehicle's mass; F_x, F_y, F_z are the resultant forces that are projected on the axes of the coordinate system fixed relative to the air vehicle. The rotational dynamics equation in the projections on a fixed coordinate system for a fixed mass and moments of inertia are described as follows:

$$\begin{cases} J_x\dot{\omega}_x + (J_z - J_y)\omega_y\omega_z &= N_x \\ J_y\dot{\omega}_y + (J_x - J_z)\omega_x\omega_z &= N_y \\ J_z\dot{\omega}_z + (J_y - J_x)\omega_x\omega_y &= N_z \end{cases} \tag{5}$$

where J_x, J_y, J_z are the air vehicle's moment of inertia with respect to the coordinate axes; N_x, N_y, N_z are the torque projection on the axes of the fixed coordinate system.

Aside from the drone, to design the control system well it needs models for the sensors connected to it and the atmosphere in which the drone operates. The sensor model is based on datasheets of the chosen sensors connected to the drone.

For the atmosphere model, there are two models used. First is a constant environment, wherein all variables such as air temperature, density, etc., are made constant. It is to control the simulation of the drone design. The variable atmosphere model was designed using three models; the World Geodetic System (WGS84), Committee on Extension to the Standard Atmosphere (COESA), and World Magnetic Model (WMM) 2015 [22]. The WGS84 model is defined as a geocentric equipotential ellipsoid. This model can be found in NIMA TR8350.2, "Department of Defense World Geodetic System 1984, Its Definition and Relationship with Local Geodetic Systems". The COESA atmosphere model calculates the atmosphere models using the 1976 COESA-extended U.S. Standard Atmosphere. Given geopotential altitude, the density, absolute pressure & temperature are obtained using standard interpolation formulas. The COESA model extrapolates pressure/density logarithmically beyond the range of 0 to 84852 *m.* (geopotential) and temperature linearly in the same geopotential range. The world magnetic model block calculates the earth's magnetic field at a specific location and time using the WMM. This model is valid for the year 2015 through the year 2020. The WMM-2015 can be found at [23] and in "NOAA Technical Report: The US/UK World Magnetic Model for 2015-2020".

C. Mapper Design

Fig. 5 shows the system architecture of the mapping system used as one of the payloads of BIRD. This payload is used for the assessment of the post-disaster response mission of BIRD. The payload is composed of a camera for image acquisition, a GPS transponder to record the drone position, an SD card to serve as the storage, and a Raspberry Pi board to serve as the main processor of the payload. The processing done in this payload is independent of the processing for the vehicle's flight.

One crucial factor that was considered in the design is its feature being a detachable payload because the BIRD includes other payloads that may be used for disaster response.

Referring to Fig. 6, the mapping payload configuration comprises two components: aerial and ground systems. The aerial mission component consisted of the payload with a digital camera with supporting modules. In contrast, the ground mission component consisted of the platform with the software that processed the captured image to develop a 2D map.

The Raspberry Pi board is used to activate the camera, capture the aerial images, and label the images. The GPS module was connected to Raspberry Pi for the latitude and longitude recording. The program in Raspberry Pi must act

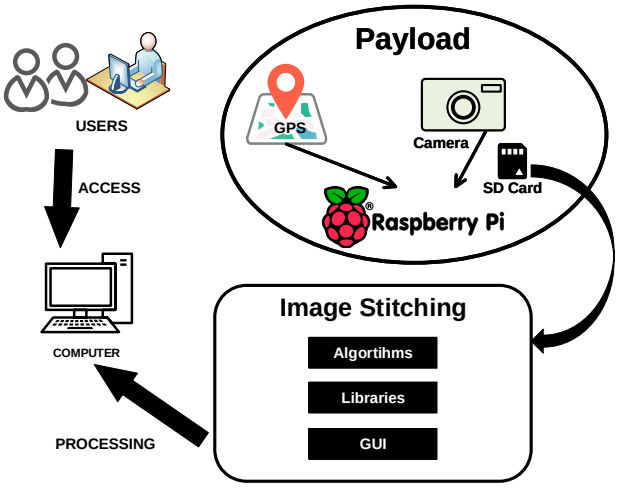

Figure 5. The system architecture of the Mapping System

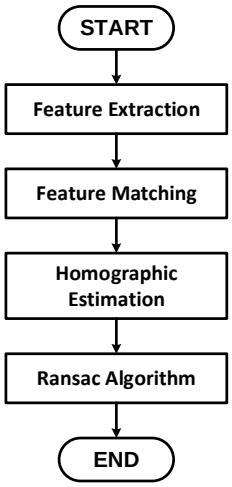

Figure 7. Image stitching flowchart

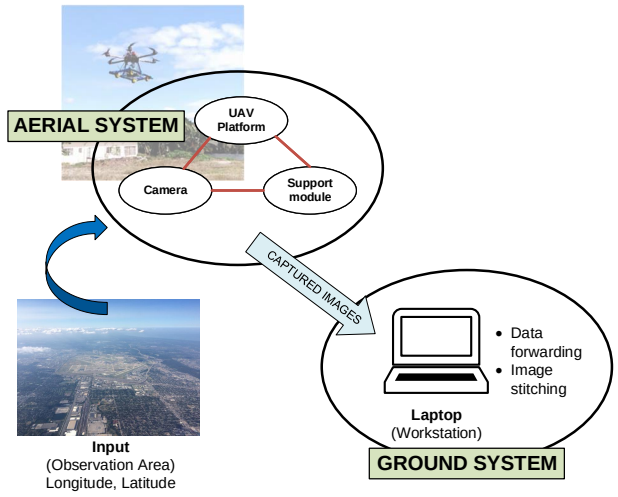

Figure 6. The system architecture of the Mapping System

as the camera's trigger to capture the image.

The ground station of the payload uses a stitching program. Several image processing techniques are used to produce a panoramic image from the captured images. Fig. 7 shows the flowchart used in image stitching.

3. Results and Discussion

A. Drone Development

Fig. 8 presents the schematic diagram of the electronic components of the unmanned aerial vehicle (UAV), including the (a) schematic diagram of the drone motor assembly, (b) unmanned ground vehicle (UGV), and (c) unmanned surface vehicle (USV). Naza M-v2 flight controller acts as the main brain of the drone. It is responsible for processing the data acquired from the receiver and its on-board sensor. The FS-ia6 receiver, electronic speed controller signal pin for motor control, and its power management unit (PMU), which has an onboard battery estimator circuit for voltage and current regulation used to power up the flight controller, were all connected in the Naza M-v2. The PMU is connected to a six-cell lithium-polymer battery wired in a series configuration. Using a power distribution board (not included in the diagram), the six electronic speed controllers were connected directly to the battery. The electronic speed controllers were linked to the six motors that provided actuation to produce enough thrust making the drone hover or glide midair. It was the receiver VCC port given that Naza M-v2 has its battery estimator circuit that powered the receiver, the X2 pin, and the servo port of Naza M-v2.

The physical structure of the drone was designed using SOLIDWORKS and material selection was made considering the different considerations, computation, and evaluation results. Fig. 9 presents the physical structure of (a) the main drone, (b) the UGV payload, and (c) the USV payload. The UGV payload consists of 4 wheels for ground navigation, while the USV payload consists of 2 motors with propellers and floaters for water navigation.

In summary, BIRD is a human-operated hexarotor drone with a weight of 3.943 *kg.* and can carry approximately 5 *kg.* of payload. It is powered by a 6S LiPo battery, with interchangeable landing gears for ground and water surfaces and a mapper payload. Table I presents the specification of BIRD.

The other electronic components like the flight controller, power management unit (PMU), etc., were placed on the top frame then the battery mount was installed above it. The battery is appropriately locked to secure and prevent it from falling or misaligning because a bit of misalignment of the battery could change the centers of mass & gravity of the hexarotor drone. Referring to Fig. 10, it shows the drone without any payloads. Fig. 11 (a) is the final assembly

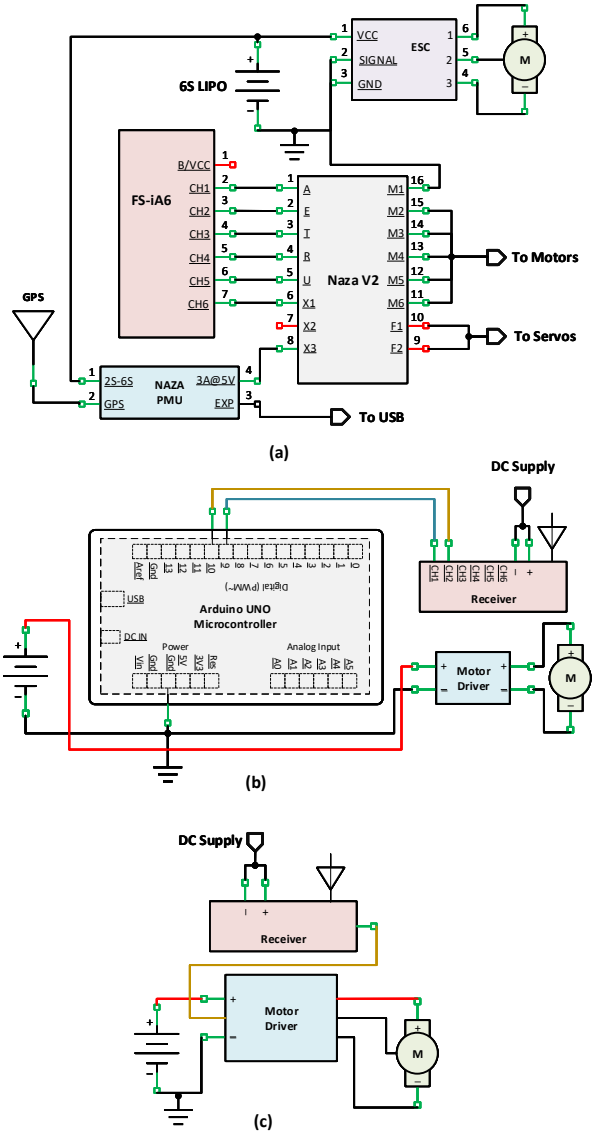

Figure 8. UAV system schematics diagram (a) Block diagram of main drone, (b) UGV configured drone and (c) USV configured drone

TABLE I. BIRD Specifications

Parameter	Values
Flight time	15 *min.*
Weight	Approx. 4 *kg.*
Max. payload weight	5 *kg.*
Max. altitude	20 *m.*
Communication	Radio frequency remote control
Payload connections	Mechanical (screws, nuts, and bolts)

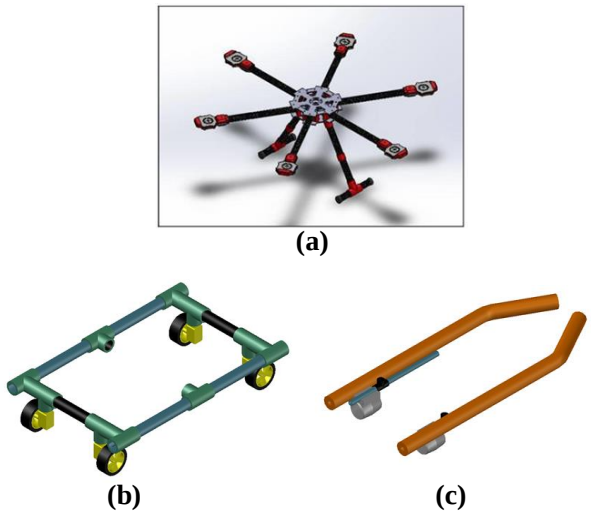

Figure 9. Drone physical structure (a) Main drone, (b) UGV payload and (c) USV payload

Figure 10. BIRD without payload

of the UGV which the drone and the ground payload are integrated. Fig. 11 (b) is the final assembly of the USV in which the drone is connected to the pay load, and electronics component that will tend to touch the water is sealed for the protection of the whole circuit.

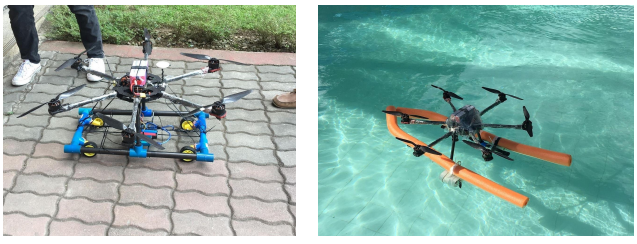

Figure 11. Actual drone (a) UGV payload and (b) USV payload

Figure 12. BIRD Simulink© SimScape© Multibody model

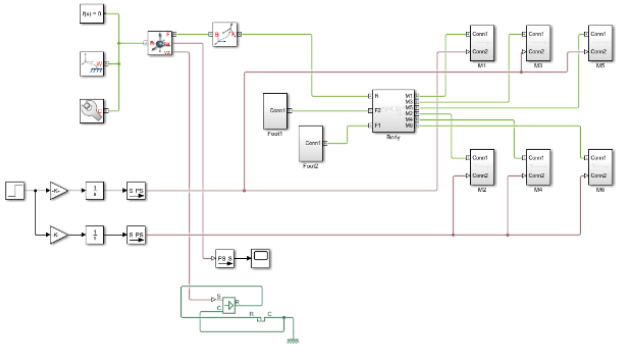

Figure 13. BIRD Simulink© SimScape© Multibody model (connections view)

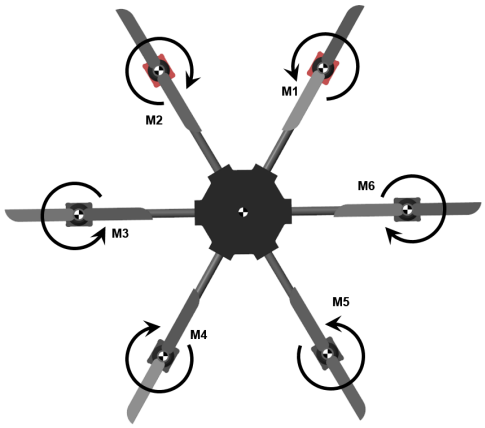

Figure 14. Motor configuration

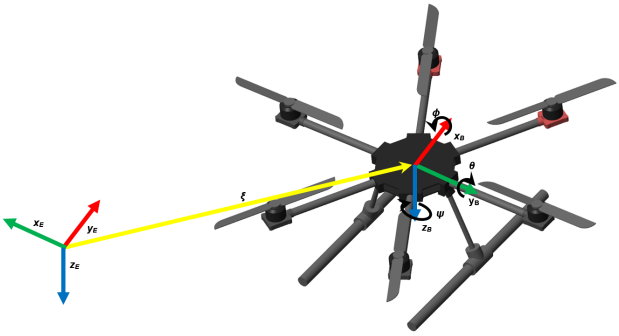

Figure 15. Reference frames

B. Plant Model

The model of the plant of the system is developed in Simulink©. Instead of creating the drone model from scratch in Simulink©, the authors used SOLIDWORKS to model the different parts of the drone. Some parts of the drones are the same; thus, creating a single model is also advantageous. There are six parts of the model drawn in SOLIDWORKS. It was then saved as a Standard for the Exchange of Product Data (STEP) file for a better import to Simulink©. Fig. 12 shows the connected parts in Simulink© Simscape© Multibody. Fig. 13 shows the connections made to create the fully connected drone.

C. Control System Model

Since the drone is already identified as a hexarotor, the next thing decided is the motor configuration used for the vehicle.

There are several configurations of a hexarotor drone. Still, there are only two symmetrical drones, the conventional design more commonly known to enthusiasts as the "+" configuration and the cant-angle hexacopter. A conventional hexacopter has all of its six rotors fixed in the body frame and thrust upwards, giving it a decoupled four-degrees- of-freedom (4DOF) motion or a coupled six-degrees-of-freedom (6DOF) motion. While a cant-angle hexacopter has all rotors canted at an angle tangent to the radius of the frame, thus providing it two degrees of freedom in the translational x and y-axis without any coupling [24].

A cant-angle hexacopter design is more suited for surveillance, mapping, ground inspection and other applications requiring maneuverability without sacrificing stability. Since the BatState-U Integrated Response will primarily be used for surveillance and mapping, the cant-angle hexacopter design is chosen.

Fig. 14 shows the motor configurations of the drone, and Fig. 15 shows the reference frame used in modeling the physics of motion of the drone.

The forces and torques that act on the hexacopter are the gravitational pull, aerodynamic forces, air friction, and torques produced from the propellers & the propeller rotation, resulting in gyroscopic effects. The torque caused by the angular acceleration of the propeller is assumed negligible. All quantities are expressed in the body-fixed frame unless otherwise stated. The contribution of the gravitational force in the body, denoted by $\mathbf{F}_E^B$, presented in (6)

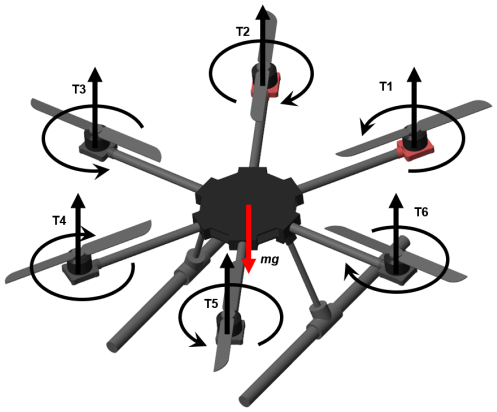

Figure 16. Torque directions and gravity effect

$$\mathbf{F}_E^B = R_L \begin{bmatrix} 0 \\ 0 \\ mg \end{bmatrix} = mg \begin{bmatrix} s\theta \\ s\phi c\theta \\ c\phi c\theta \end{bmatrix} \tag{6}$$

where g is the acceleration due to gravity, R_L is the rotation matrix of the drone with respect to earth. The notations $s\theta$, $s\phi$, $c\theta$, and $c\phi$ means $\sin\theta$, $\sin\phi$, $\cos\theta$, and $\cos\phi$, respectively.

The lift force can be denoted by, F_w, can be determined by (7).

$$F_w = \begin{bmatrix} 1 & 1 & 1 & 1 & 1 & 1 \end{bmatrix} (T) \tag{7}$$

where

$$T = \begin{bmatrix} T_1 \\ T_2 \\ T_3 \\ T_4 \\ T_5 \\ T_6 \end{bmatrix}$$

Since the propellers, the sources of thrust, are not located in the center of gravity, torques are created around the different axes of rotation. Around the x_B-axis the torques M_p from propeller thrust is presented in .

$$M_p = \begin{bmatrix} -\frac{\sqrt{3}}{2} & \frac{\sqrt{3}}{2} & 1 & \frac{\sqrt{3}}{2} & -\frac{\sqrt{3}}{2} & -1 \end{bmatrix} (l)(T) \tag{8}$$

where l is the length of each arm. Around the y_B-axis, the torques M_q shown in (9).

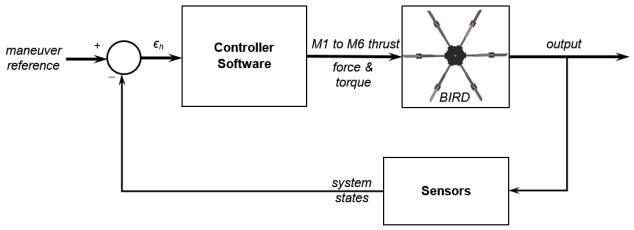

Figure 17. Initial control architecture

$$M_q = \begin{bmatrix} \frac{1}{2} & \frac{1}{2} & 1 & -\frac{1}{2} & -\frac{1}{2} & -1 \end{bmatrix} (l)(T) \tag{9}$$

The torque around the z_B –axis is a result of Newton's third law. When the motor accelerates and keeps the propeller rotating, it exerts a torque on the propeller shaft. The motor will be subjected to an equally sized torque opposite from the propeller shaft. Since the motor is mounted to the airframe, the torque will propagate. This torque is often called reaction torque. If the reaction torque from the propeller is called τ, the total torque around the z_B-axis denoted M_r is

$$M_r = \sum_{i=1}^{6} (-1)^{i+1} \tau_i$$

where

$$\tau = \begin{bmatrix} \tau_1 \\ \tau_2 \\ \tau_3 \\ \tau_4 \\ \tau_5 \\ \tau_6 \end{bmatrix} = \frac{c_q}{c_t} l \cdot T$$

Now,

$$M_r = \begin{bmatrix} 1 & -1 & 1 & -1 & 1 & -1 \end{bmatrix} \left(\frac{c_q}{c_t} \right) (T) \tag{10}$$

The control architecture is designed using an iterative and intuitive method. Since there are four hexacopter movements, the controller was designed to accommodate these four movements. Fig. 17 is the initial architecture considered for the control system.

The hexacopter must adjust its movement should there be any outside disturbances. A motor mixing algorithm should be in the controller loop to perform roll, pitch, and yaw correction to maintain a level flight. Fig. 18 shows the block diagram considered for the altitude control system. In this diagram, it is assumed that the roll and pitch angles

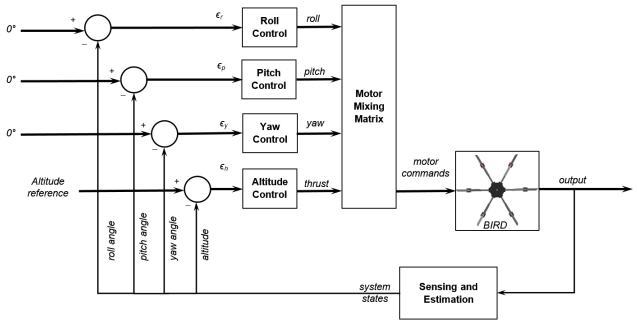

Figure 18. Roll, pitch, yaw, and altitude control

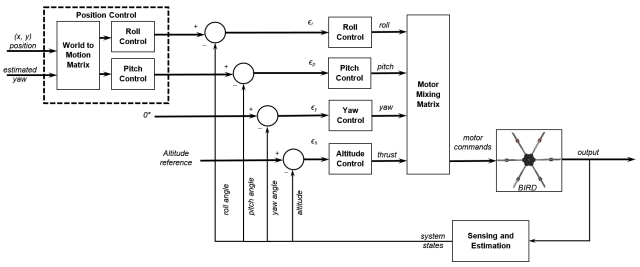

Figure 19. Control architecture with position control

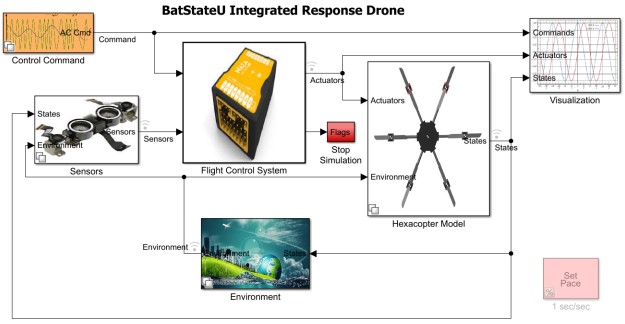

Figure 20. BIRD Top-Level Model

TABLE II. Effect of Flight Style in Flight Time

Trial No.	Flying Style	Time (sec)
1	Hover	1074
2	Hover	1065
3	Hover	1051
4	Glide	662
5	Glide	646
6	Glide	654

are so small that they will have no or very minimal effect on the altitude of the hexacopter.

The diagram presented in Fig. 18 does not consider changing positions. It may control the roll and pitch angles; however, that may cause the hexacopter to change positions. It will be better if a position reference outside the control loop is connected to maintain the position of the hexacopter. The position controller takes the estimated roll, pitch, and yaw of the hexacopter and converts it to the reference roll and pitch angles for the controller in the loop. The final control architecture with position control is shown in Fig. 19.

Fig. 20 shows that the top model comprises six different parts; flight control system, hexacopter model, sensors, environment, control commands, and visualization. The flight control system is the main focus of this study, and it is the algorithm implemented in the hexacopter. All the other blocks are there to provide the flight control system with a near realistic simulation. The hexacopter model subsystem is used to simulate the dynamic characteristics of the hexacopter; it is modeled from the rotor characteristics and the equations of motion of the hexacopter. The environment subsystem includes models of the environment that might affect the performance of the hexacopter. The sensors subsystem is a model of how the sensors work. The control and the visualization subsystems are used to feed in and visualize signals from the simulation.

The state estimator inside the controller is designed to estimate the states on which the hexacopter is. It shows the relative position, velocity, acceleration, roll angle, pitch angle, and yaw angle of the hexacopter. This block uses Kalman filters to compute the needed estimated values. It is composed of the sensor preprocessing unit, a complementary filter, an attitude estimator, and the position estimator.

After creating the entire model, the controllers were tuned using MATLAB© Control Systems toolbox. The gains of the PID blocks used are tuned using the PID tuner app. Fig. 21 and 22 shows the results of the simulations after tuning the controller.

D. Flight Test

The flight time is affected by the battery capacity, weight, and flying style. Table II shows how flying style affects the flight time. The battery capacity and weight were constant while the throttle was maintained at 70% and two flying styles, hovering & gliding were tested.

Table III shows the result of testing BIRD outdoor during daytime using the UGV payload.

Both UGV and USV payloads were tested by navigating their forward, reverse, left, and right functions. Fig. 23 shows the UAV during flight. Referring to Fig. 24, shows a sample hover test. The drone was given a command to

TABLE III. BIRD Outdoor Testing

Trial Number	Time (sec)	Stability (in air)	Remarks
1	30	Stable	Hard Landing
2	38	Stable	Soft Landing
3	58	Stable	Soft Landing

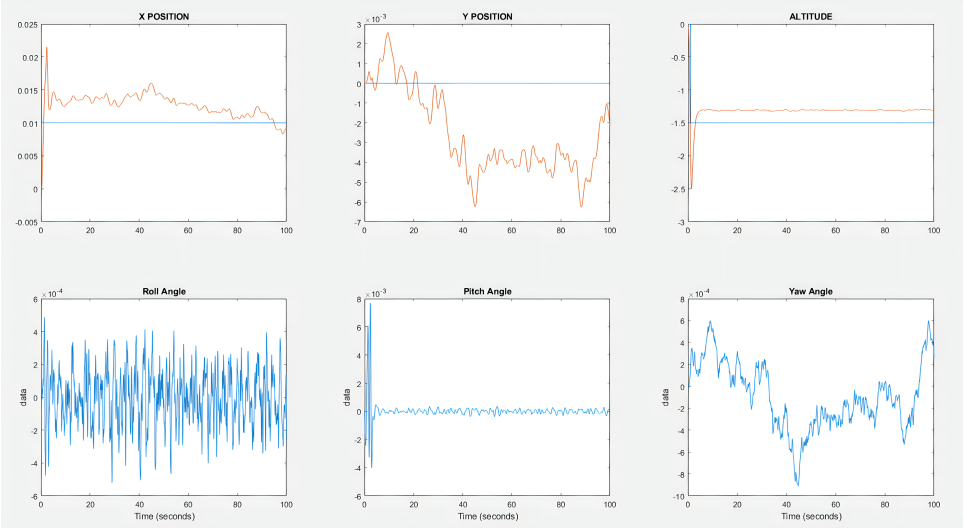

Figure 21. Simulation result (hovering)

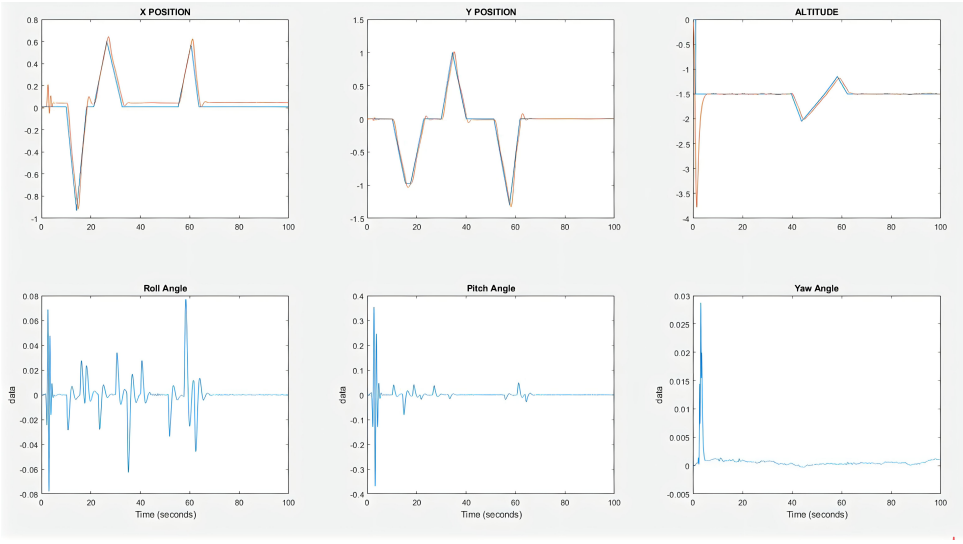

Figure 22. Simulation result (xyz-movement)

hover at 1.5 *m.* height, it can be seen that before achieving a steady-state the drone reached a height of 1.8 *m.* From this, the drone can be said to behave like a second-order underdamp system.

To be able to verify the functionality of the controller before deployment to an outdoor test, an indoor test is required. The laboratory in which the drone is tested is a closed room and the airflow inside is almost negligible to affect the drone's movement. For each test, the battery is maintained to always be more than 70% charged. Three test coordinates, not including an origin point O(0, 0, 0), are identified to test the performance of the drone controller, namely 1. Point A(0, 0, 1), 2. Point B(1, 0, 1), and 3. Point C(1, 1, 1). Note that this notation assumes a coordinate unit of 1 *m.* These points are the reference for the step response approximation of the controller. To test the altitude (z) control of the drone, the command sequence of the drone is from Point O to Point A. For the x and y movement, the sequence is from Point A to Point B and from Point B to Point C, respectively. The sequences are tested 50 times to get the approximate response of the controllers. This is to minimize the human errors performed during the simulations. Another test is performed for the x-y movement. The measurements are done using the sequence from Point O, then Point A, and then Point C.

The same test sequences are done outside the laboratory to see how the controllers react to disturbances. In these tests, the battery is maintained again at least 70%. Since the target deployment of the drone is for the post-disaster response it is critical that the drone can least withstand

Figure 23. UAV during flight

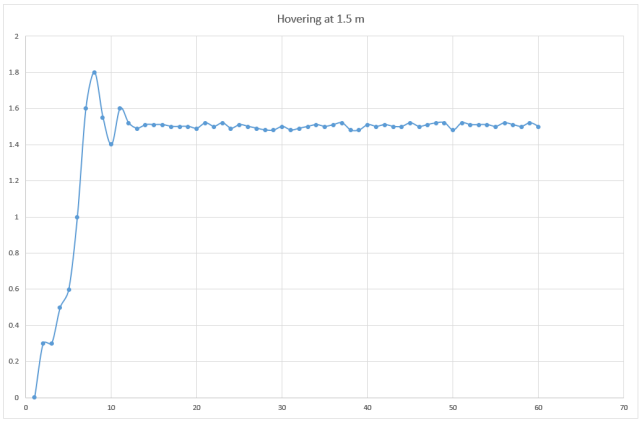

Figure 24. Hovering test at 1.5 *m.* height

at least 10 *m/s* wind speed, which is a bit more that the minimum Signal No. 1 typhoon wind speed. Hence, all outdoor tests are done when the wind speed is between 5 to 10 *m/s*.

All tests are repeated 10 more times when the drone is configured as a UGV and as a USV. There is no significant difference with the different control parameters tested prior. A noticeable change for the UGV configuration is the final position after landing. The front facing pose shifted at an approximate ±10°. This is because the weight of the landing gear is not in the center of inertia. Also, some the landings by the UGV configuration is not consistent, sometimes it landed softly while sometimes it lands hard, as shown in Table III. For the USV configuration, the take-off time was observed to be slower by around 1 second.

Table V summarizes the simulation, indoor, and outdoor controller test using the above-mentioned setup. The result shows that the drone achieves the design parameters intended for drone movement. It can be noticed in the table that the xy-control outdoor test sometimes achieves results that is beyond the target. Since the control is designed for singular movement it is expected that the controller will sometimes behave like that.

TABLE IV. Summary of Materials

UAV- Unmanned Aerial Vehicle Configuration
Carbon fiber propeller
Customized carbon fiber frame
MT4114 340KV Outrunner Brushless Motor
YPG 6S 5200mAh 40C LiPo Battery
Carbon fiber arm
Motor mount
Landing gear
Hobbywing Platinum 30A Pro 2-6S ESC OPTO
DJI NAZA-M + GPS V2 (GPS & MC)
UGV- Unmanned Ground Vehicle Configuration
Motor Driver L298-N
Arduino Uno
5 V, 2 A, 30 Ah Power Bank
FS-iA6 receiver
18650 Li-ion Battery
120:1 gearmotor
3D Printed connectors
DC motors with robot car wheel
USV- Unmanned Surface Vehicle Configuration
Emax Brushless Motor – XA2212 820kV
HobbyWing X-rotor 40A opto ESC
Fs-iA6 receiver
3S Battery
Floater
3D Printed connectors
Mapper Payload
5 V, 2 A, 20.8 Ah Power Bank
3D Printed case and connectors
Nikon Coolpix AW100 16 Megapixel Camera

4. Conclusions and Future Works

The BatStateU Integrated Response Drone (BIRD) is a hexacopter drone that consists of a mapper payload that can be attached and removed mechanically. The mapper payload is used to take pictures and stitch them together to form a single picture. It also has two additional landing gears for different terrain. The design was constructed using software such as MATLAB, SOLIDWORKS, and AutoCAD with several equations. The hexacopter was developed using carbon fiber materials for the frame, motor MT 4114, with the weight of thrust force has a maximum value of -1.8547 *kN* or -1854.7 *N*, with an angular velocity of 565 *rad/s*. The drone was tested for its control parameters through simulation, indoor, and outdoor tests. Results from the actual test found a significant difference in the performance of the drone. This can be taken into account from the

TABLE V. Indoor and Outdoor Control Test Results

Control	Overshoot (%) (max. 35%)			Rise Time (s) (at least 10 s)			S.S. Error (%) (max. 10%)		
	S[1]	I[2]	O[3]	S[1]	I[2]	O[3]	S[1]	I[2]	O[2]
z-control[a] (Altitude)	8	15 22 2	16 29 5	4	7 10 5	8 10 6	2	4 6 3	6 8 3
x-control[b]	3	14 28 2	18 33 8	4	6 9 4	7 9 5	3	6 9 3	6 11 5
y-control[c]	3	12 27 4	17 29 8	3	7 9 5	7 9 5	3	5 9 4	6 12 4
xy-control[d]	5	15 24 5	19 33 10	4	9 12 7	10 15 8	4	9 10 8	10 14 8

[1]S- Simulation
[2]I- Indoor Test (Ave., Max., Min.)
[3]O- Outdoor Test (Ave., Max., Min.)
[a] P(0, 0, 0) → $A(0, 0, 1)$
[b] A(0, 0, 1) → B(1, 0, 1)
[c] B(1, 0, 1) → C(1, 1, 1)
[d] P(0, 0, 0) → A(0, 0, 1) → C(1, 1, 1)

TABLE VI. Comparison with other disaster response drones

	Type	**Flight Processor**	**Controller and Sensors**	**Operation**	**Payload**	**Application**
2020 [25]	Quadrotor	PSoC/ RX621	Extended Kalman Filter/ PID, ultrasonic sensor, GPS	Manual	PlayStation Eye and Loudspeaker	search operations using sound
2019 [13]	Hexacopter	Raspberry Pi 3	GPS, IMU	Autonomous	Camera and AI system with Lifebuoy	search and rescue at sea
2019 [14]	Fixed-wing	DJI Phantom 4	PID, GNSS, barometric altitude, airspeed indicator, IMU	Autonomous	Geiger-Muller tubes and SIGMA-50 detectors	radiation mapping
2019 [9]	Quadrotor	Arduino	GPS, Temperature	Manual	Telemedicine	used for delivery of small medical equipment
This work	Hexacopter	Naza-M v2 and Raspbery Pi	Extended Kalman Filter, Complementary Filter, PID, GPS, altimeter, temperature, IMU	Manual and Semi-autonomous	different landing gears, mapper system	used for search and rescue, can be used to deliver small things up to 5 kg

disturbances that are present during the actual test. The worst overshoot was found to be 33% which was 2% lower than the maximum design target. The drone motion control is found to have a maximum rise time of 15 s and a maximum steady-state error of 14%. The drone can be configured to be a UAV, hybrid UAV-USV, and hybrid UAV-USV. Landing positions were affected when the drone is configured as hybrid UAV-UGC, while take-off time was longer when configured as hybrid UAV-USV.

The BIRD project is capable to be deployed during actual post-disaster operations. The next step for the authors is the licensing of the drone to be used in the air space of the Philippines. Additional payloads are being developed to improve the mission capability of the drone. These include the design of a telemedicine payload, which can be used to deliver small medical equipment. A point-to-point communication system using SDR (software-defined radio) can also be used as a payload to provide a communication link between affected areas after a disaster.

Appendix

TABLE VII. Symbols Used

Symbol	Parameter
F_{lift}	propeller lift force
ρ	air density
v_e	air exit velocity at propeller
v_o	air entry velocity at propeller
x_B, y_B, z_B	UAV's coordinates
$A(\psi, \theta, \phi)$	UAV's rotation coordinates
ψ	yaw angle
θ	pitch angle
ϕ	roll angle
ω_x, ω_y, ω_z	UAV's angular velocities
V_x, V_y, V_z	linear speed components
F_x, F_y, F_z	resultant forces
J_x, J_y, J_z	moments of inertia
N_x, N_y, N_z	torque projections
R_L	rotation matrix with respect to earth
F_w	UAV lift force
T	thrust matrix
l	UAV arm length
τ	reaction torque matrix
c_q, c_t	drag coefficients
M_p	torque around x_B-axis
M_q	torque around y_B-axis
M_r	torque around z_B-axis

Acknowledgment

The authors are grateful to the different research centers (MRC, ESRC, and GADC) of Batangas State University for their support of BIRD project. We would like to thank the Manufacturing Research Center (MRC) for the services in the fabrication of 3D printed materials, the Electronic Systems Research Center (ESRC) for the support in electronic testing & prototyping, and the GIS Applications and Development Center (GADC) for the support in the mapper simulation and design.

References

[1] IFRC. World Disasters Report 2020. [Online]. Available: https://www.ifrc.org/document/world-disasters-report-2020

[2] WEF. Global Risks Report 2022. [Online]. Available: https://www3.weforum.org/docs/WEF_The_Global_Risks_Report_2022.pdf

[3] S. Chowdhury, A. Emelogu, M. Marufuzzaman, S. G. Nurre, and L. Bian, "Drones for disaster response and relief operations: A continuous approximation model," *Int. J. Production Econ.*, vol. 188, pp. 167–184, Jun. 2017.

[4] S. M. S. M. Daud, M. Y. P. M. Yusof, C. C. Heo, L. S. Khoo, M. K. C. Singh, M. S. Mahmood, and H. Nawawi, "Applications of drone in disaster management: A scoping review," *Sci. Justice*, vol. 62, no. 1, pp. 30–42, Jan. 2022.

[5] T. Luege. Case Study No 9: Using Drone Imagery for real-time information after Typhoon Haiyan in The Philippines. [Online]. Available: https://europa.eu/capacity4dev/innov-aid/discussions/

[6] P. Meier. The Use of Expendable UAVs After Typhoon Haiyan. [Online]. Available: https://irevolutions.org/2014/06/10/expendable-uavs-typhoon-haiyan/

[7] J. M. Teixeira, R. Ferreira, M. Santos, and V. Teichrieb, "Teleoperation using google glass and AR, drone for structural inspection," in *Proc. 2014 XVI Symp. Virtual Augmented Reality*. IEEE, May 2014.

[8] S.-S. Choi and E.-K. Kim, "Building crack inspection using small UAV," in *Proc. 2015 17th Int. Conf. Adv. Commun. Technol. (ICACT)*. IEEE, Jul. 2015.

[9] R. S. Vaishali Nimilan, Gunaselvi Manohar and P. Stanley, "DroneAid: An aerial medical assistance," *Int. J. Innovative Technol. Exploring Eng.*, vol. 8, no. 11S, pp. 1288–1292, Oct. 2019.

[10] C. Alex and A. Vijaychandra, "Autonomous cloud based drone system for disaster response and mitigation," in *Proc. 2016 Int. Conf. Robot. Automat. Humanitarian Appl. (RAHA)*. IEEE, Dec. 2016.

[11] J. Colorado, C. Devia, M. Perez, I. Mondragon, D. Mendez, and C. Parra, "Low-altitude autonomous drone navigation for landmine detection purposes," in *Proc. 2017 Int. Conf. Unmanned Aircr. Syst. (ICUAS)*. IEEE, Jun. 2017, pp. 540–546.

[12] A. L. P. de Ocampo, A. A. Bandala, and E. P. Dadios, "Coverage path planning on multi-depot, fuel constraint UAV missions for smart farm monitoring," in *Proc. 2018 IEEE Region Ten Symposium (TenSymp)*. IEEE, Jul. 2018, pp. 13–18.

[13] E. Lygouras, N. Santavas, A. Taitzoglou, K. Tarchanidis, A. Mitropoulos, and A. Gasteratos, "Unsupervised human detection with an embedded vision system on a fully autonomous UAV for search and rescue operations," *Sensors*, vol. 19, no. 16, pp. 3542–1~20, Aug. 2019.

[14] D. T. Connor, K. Wood, P. G. Martin, S. Goren, D. Megson-Smith, Y. Verbelen, I. Chyzhevskyi, S. Kirieiev, N. T. Smith, T. Richardson, and T. B. Scott, "Radiological mapping of post-disaster nuclear environments using fixed-wing unmanned aerial systems: A study from chornobyl," *Frontiers Robot. AI*, vol. 6, Jan. 2020.

[15] V. Artale, A. Ricciardello, and C. Milazzo, "Mathematical modeling of hexacopter," *Appl. Math. Sci.*, vol. 7, pp. 4805–4811, Jul. 2013.

[16] M. S. Islam, M. M. Hasan, M. M. A. K. Tamal, M. J. Mian, and M. T. R. Evan, "Detail Solidworks design and simulation of an unmanned air vehicle," *IOSR J. Mech. Civil Eng.*, vol. 8, pp. 95–100, Oct. 2013.

[17] W. Grodzki, A. Łukaszewicz, and K. Leśniewski, "Modelling of UAV's composite structures and prediction of safety factor," *Appl. Comput. Sci.*, vol. 11, no. 3, pp. 67–75, Oct. 2015.

[18] F. Cocchioni, A. Mancini, and S. Longhi, "Autonomous navigation, landing and recharge of a quadrotor using artificial vision," in *Proc. 2014 Int. Conf. Unmanned Aircr. Syst. (ICUAS)*. IEEE, May 2014, pp. 418–429.

[19] V. Babu, D. K. Das, and S. Kumar, "Designing of self tuning PID controller for AR drone quadrotor," in *Proc. 2017 18th Int. Conf. Adv. Robot. (ICAR)*. IEEE, Jul. 2017, pp. 167–172.

[20] G. P. Falconí, J. Angelov, and F. Holzapfel, "Hexacopter outdoor flight test results using adaptive control allocation subject to an unknown complete loss of one propeller," in *Proc. 2016 3rd Conf. Control Fault-Tolerant Syst. (SysTol)*. IEEE, Sep. 2016, pp. 373–380.

[21] S. Kiga, S. Ouchi, N. Hasebe, N. Kodani, Y. Takamoto, and M. Mubin, "Attitude control of drones by back-stepping controller," in *Proc. 2017 56th Ann. Conf. Soc. Instrum. Control Engineers Jpn. (SICE)*. IEEE, Sep. 2017, pp. 25–30.

[22] U.S. Standard Atmosphere 1976. [Online]. Available: https://ccmc.gsfc.nasa.gov/modelweb/atmos/us_standard.html

[23] The World Magnetic Model. [Online]. Available: https://www.ngdc.noaa.gov/geomag/WMM/

[24] H. Das, "A comparative study between a cant angle hexacopter and a conventional hexacopter," in *Proc. 2016 Int. Conf. Control, Instrum., Commun. Computational Technol. (ICCICCT)*. IEEE, Dec. 2016.

[25] Y. Yamazaki, C. Premachandra, and C. J. Perea, "Audio-processing-based human detection at disaster sites with unmanned aerial vehicle," *IEEE Access*, vol. 8, pp. 101 398–101 405, Jun. 2020.

Ralph Gerard B. Sangalang received his B.S. degree in Electronics and Communications Engineering and M.S. in Electronics Engineering at Batangas State University. He is currently pursuing his Ph.D. in Electronics Engineering and Ph.D. in Electrical Engineering under the double degree program at Batangas State University and National Sun Yat-Sen University. He has been with Batangas State University since 2009 and was the Student Outcome Committee Chair of the College of Engineering, Architecture and Fine Arts. He was also the former Program Chair of Electronics Engineering. His research interests includes memory design, digital systems, control systems, computational modeling, fractional circuits, and engineering education.

Oliver Lexter July A. Jose received his B.S. degree in Electronics and Communications Engineering at De La Salle-Lipa and M.S. in Electronics Engineering at Batangas State University. He is currently pursuing his Ph.D. in Electronics Engineering and Ph.D. in Electrical Engineering under the double degree program at Batangas State University and National Sun Yat-Sen University.

Antonette V. Chua received her B.S. degree in Electronics and Communications Engineering at South Luzon State University and M.S. in Electronics Engineering at Batangas State University. She is currently pursuing her Ph.D. in Electronics Engineering at Batangas State University. She was formerly the Program Chair of BS Electronics Engineering and BS Biomedical Engineering at Batangas State University. She is a Huawei Certified Internet Associate (HCIA) and Huawei Certified Academy Instructor (HCAI).

Janice F. Peralta received her B.S. degree in Electronics and Communications Engineering and M.S. in Electronics Engineering at Batangas State University. She is currently pursuing her Ph.D. in Electronics Engineering at Batangas State University. She was formerly the Center Head of the GIS Applications Development Center of Batangas State University. She is a Huawei Certified Internet Associate (HCIA), Huawei Certified Academy Instructor (HCAI), and a Certified Google Educator Level 1 and 2.